Electronic Supplementary Material (ESI) for Food & Function.
This journal is © The Royal Society of Chemistry 2021

Supplementary Material

A systematic study on the chemical diversity and efficacy of inflorescence and succulent stem of *Cynomorium songaricum*

Yan Zheng[1,2], Sun Xiao[1], Yujing Miao[1], Shunwang Qin[3], Yuan Jiang[1,4], Xiang Zhang[1], Linfang Huang[1*]

1 Key Laboratory of Chinese Medicine Resources Conservation, State Administration of Traditional Chinese Medicine of the People's Republic of China, Institute of Medicinal Plant Development, Chinese Academy of Medical Sciences & Peking Union Medical College, Beijing, China

2 Jiangxi University of Traditional Chinese Medicine, Nanchang, Jiangxi, China

3 Chengdu University, Chengdu, Sichuan, China

4 Dali University, Da Li, Yun Nan, China

Yan Zheng: zhengyan6886@163.com

*Correspondence:

Linfang Huang: lfhuang@implad.ac.cn;

Supplement methods

1. ESI-Q TRAP-MS/MS

LIT and triple quadrupole (QQQ) scans were acquired on a triple quadrupole-linear ion trap mass spectrometer (Q TRAP, API 6500 Q TRAP LC/MS/MS System) equipped with an ESI Turbo Ion-Spray interface. It was operated in a positive ion mode and controlled by Analyst 1.6.3 software (AB Sciex). The ESI source operation parameters were as follows: ion source, turbo spray; source temperature 500 ℃; ion spray voltage, 5500 V; ion source gas I (GSI), gas II (GSII), and curtain gas was set at 55, 60, and 25.0 psi, respectively; collision gas was high. Instrument tuning and mass calibration were performed with 10 and 100 μmol/L polypropylene glycol solutions in QQQ and LIT modes, respectively. QQQ scans were acquired as MRM experiments with collision gas (nitrogen) set to 5 psi. DP and CE for individual MRM transitions were done with further DP and CE optimization. A specific set of MRM transitions were monitored for each period according to the metabolites eluted within this period.

2. Molecular docking method

2.1 Ligand preparation

AutoDock Vina accept files only in PDBQT file format. The docking GUI frontend PyRx was applied to prepare all protein and compound files for molecular docking, which was also employed to produce docking parameter input files. Therefore, the target and ligand must be converted into PDBQT format by PyRx tool (AutoDock Ligand) [1].

2.2 Molecular docking

AutoDock Vina [2] were used for the molecular docking studies. Positive compounds, compounds, and three protein targets were loaded into PyRx (Python 2.6.5) 0.8 with the incorporation of Autodock vina. For each of the docking steps, the OpenBabel [3] was used to import the ligands, which is a plug-in tool in PyRx 0.8. The ‘Maximize’ option in PyRx was used to define the docking boxes around the targets, since it could ensure the availability of the entire protein surface and accessible interior pockets for potential binding of ligands during ‘blind’ docking. For the 3 protein targets, the Dimensions (Angstrom) of ALB is X:79.8647, Y:107.4559, and Z:78.8741. The Dimensions (Angstrom) of MPO target Dimensions (Angstrom) is X:81.7875, Y:87.7630, and Z:104.8763. The Dimensions (Angstrom) of NOS_2 Dimensions (Angstrom) is X:147.8857, Y:85.1181, and Z 133.2018.

The default exhaustiveness value of 8 was set for all molecular dockings. The

compounds were then ranked by their binding energies. The dockings were performed by specifying fixed structures for protein receptors, whereas the ligands were semi-rigid with full torsional flexibility. The Intel Xeon Sandy Bridge 2.6 GHz Broadwell nodes of the high-performance computing cluster located at the National Computational Infrastructure (Canberra, Australia) was used to conduct Autodock Vina calculations [4]. All the other parameters were kept as default. After the completion of the docking process, the binding affinities of the protein for the compounds for the selected clusters were recorded in Table S9 and S10.

Reference:

1. S. Dallakyan and A. J. Olson, Small-Molecule Library Screening by Docking with PyRx, *Methods in Molecular Biology*, 2015, **1263**, 243.
2. O. Trott and A. J. Olson, Software news and update AutoDock Vina: Improving the speed and accuracy of docking with a new scoring function, efficient optimization, and multithreading, *Journal of Computational Chemistry*, 2010, **31**, 455-461.
3. N. M. O'Boyle, M. Banck, C. A. James, C. Morley and G. R. Hutchison, Open Babel: An open chemical toolbox, *Journal of Cheminformatics*, 2011, **3**, 33.
4. H. Li, A. Hung and A. Yang, Herb-target virtual screening and network pharmacology for prediction of molecular mechanism of Danggui Beimu Kushen Wan for prostate cancer, *Scientific Reports*, 2021, **11,** 6656.

Supplementary figures

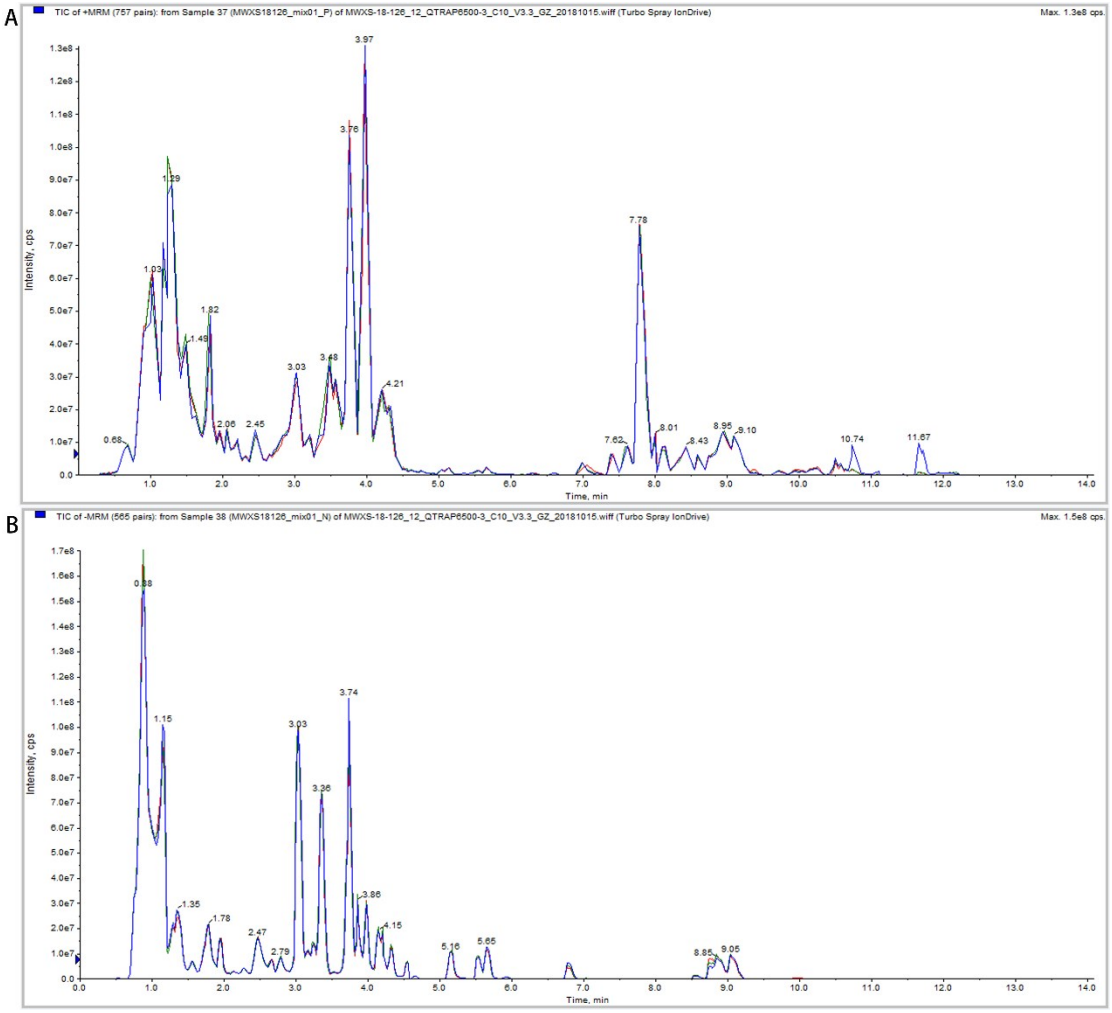

Figure S1. QC sample mass spectrometry detection TIC overlay image. (A) Positive ion current of one quality control sample by mass spectrometry detection. (B) Negative ion current of one quality control sample by mass spectrometry detection

Note: the superposition diagram of the total ion flow map (TIC) detected by QC sample mass spectrometry. The results showed that the curve overlap of metabolite detection of total ion current was high, that is, the retention time and peak intensity were the same, indicating that the signal stability was good when the same sample was detected by mass spectrometry at different time. The high stability of the instrument provides an important guarantee for the repeatability and reliability of the data.

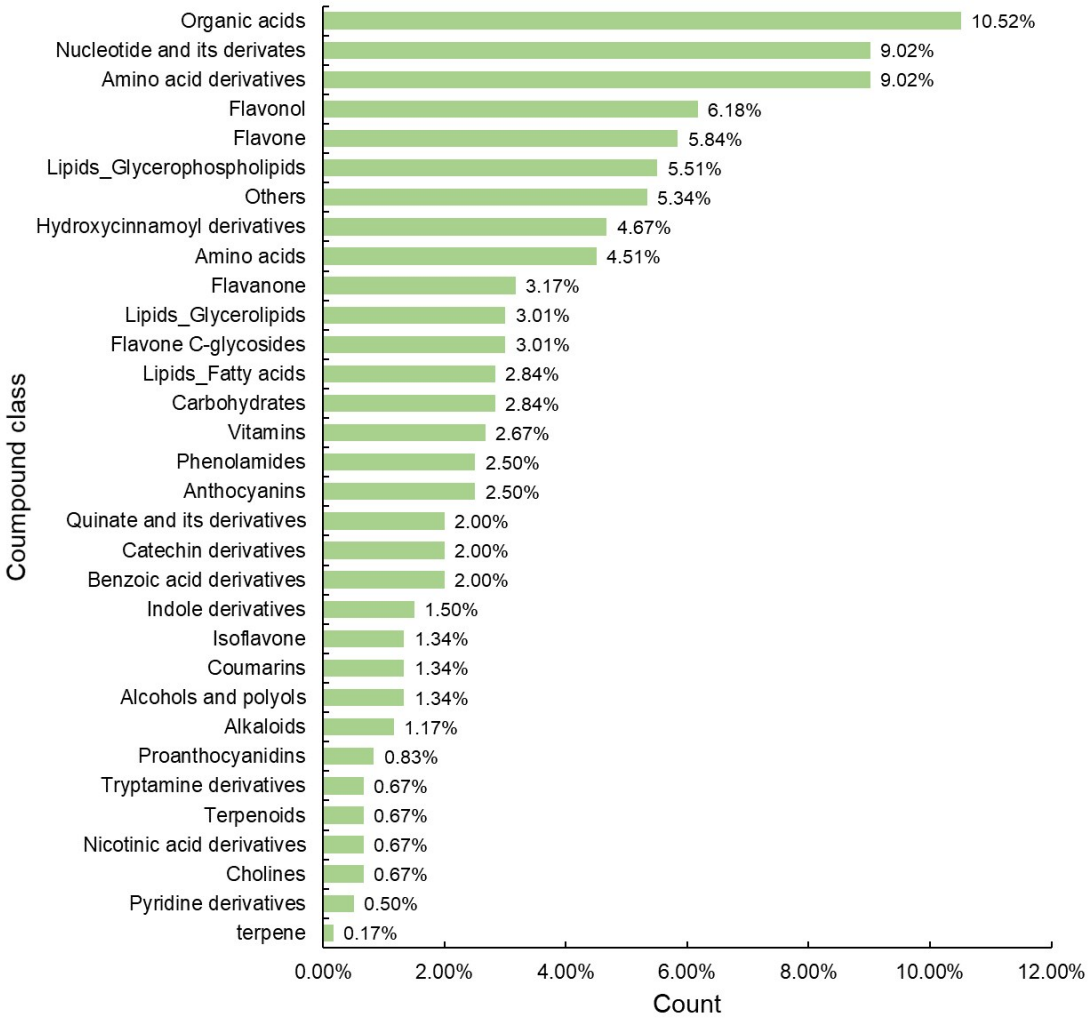

Figure S2. The compound class of succulent stem and inflorescence of *C. songaricum*.

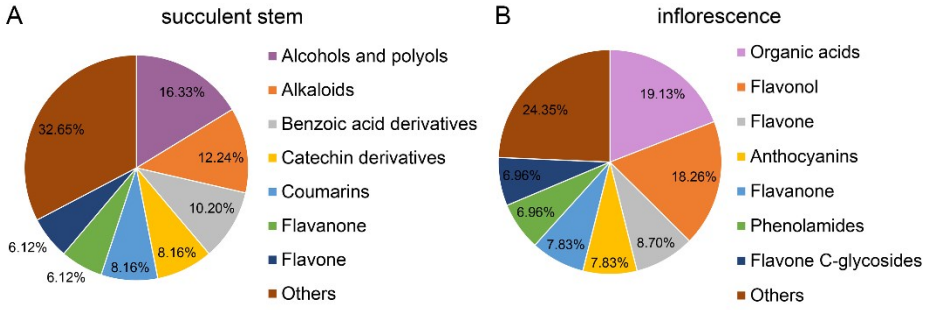

Figure S3. Types of metabolites in succulent stem and inflorescence. (A) Types of metabolites in the succulent stem; (B) Types of metabolites in the inflorescence.

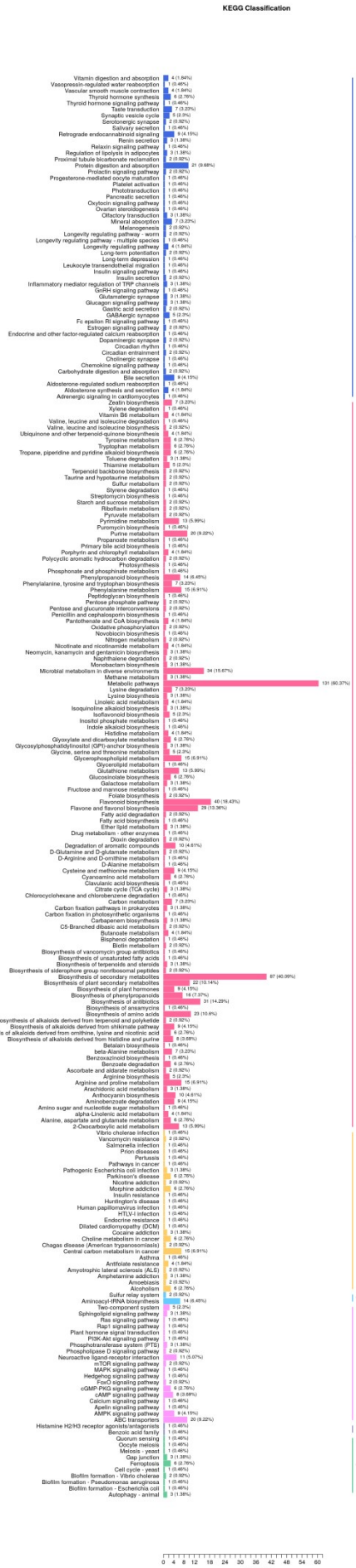
KEGG Classification
Vitamin digestion and absorption 4 (1.84%)
Vasopressin-regulated water reabsorption 1 (0.46%)
Vascular smooth muscle contraction 4 (1.84%)
Thyroid hormone synthesis 6 (2.76%)
Thyroid hormone signaling pathway 1 (0.46%)
Taste transduction 7 (3.23%)
Synaptic vesicle cycle 5 (2.3%)
Serotonergic synapse 2 (0.92%)
Salivary secretion 1 (0.46%)
Retrograde endocannabinoid signaling 9 (4.15%)
Renin secretion 3 (1.38%)
Relaxin signaling pathway 1 (0.46%)
Regulation of lipolysis in adipocytes 3 (1.38%)
Proximal tubule bicarbonate reclamation 2 (0.92%)
Protein digestion and absorption 21 (9.68%)
Prolactin signaling pathway 2 (0.92%)
Progesterone-mediated oocyte maturation 1 (0.46%)
Platelet activation 1 (0.46%)
Phototransduction 1 (0.46%)
Pancreatic secretion 1 (0.46%)
Oxytocin signaling pathway 1 (0.46%)
Ovarian steroidogenesis 1 (0.46%)
Olfactory transduction 3 (1.38%)
Mineral absorption 7 (3.23%)
Melanogenesis 2 (0.92%)
Longevity regulating pathway - worm 2 (0.92%)
Longevity regulating pathway - multiple species 1 (0.46%)
Longevity regulating pathway 4 (1.84%)
Long-term potentiation 2 (0.92%)
Long-term depression 1 (0.46%)
Leukocyte transendothelial migration 1 (0.46%)
Insulin signaling pathway 1 (0.46%)
Insulin secretion 2 (0.92%)
Inflammatory mediator regulation of TRP channels 3 (1.38%)
GnRH signaling pathway 1 (0.46%)
Glutamatergic synapse 3 (1.38%)
Glucagon signaling pathway 3 (1.38%)
Gastric acid secretion 2 (0.92%)
GABAergic synapse 5 (2.3%)
Fc epsilon RI signaling pathway 1 (0.46%)
Estrogen signaling pathway 2 (0.92%)
Endocrine and other factor-regulated calcium reabsorption 1 (0.46%)
Dopaminergic synapse 2 (0.92%)
Circadian rhythm 1 (0.46%)
Circadian entrainment 2 (0.92%)
Cholinergic synapse 1 (0.46%)
Chemokine signaling pathway 1 (0.46%)
Carbohydrate digestion and absorption 2 (0.92%)
Bile secretion 9 (4.15%)
Aldosterone-regulated sodium reabsorption 1 (0.46%)
Aldosterone synthesis and secretion 4 (1.84%)
Adrenergic signaling in cardiomyocytes 1 (0.46%)
Organismal Systems
Zeatin biosynthesis 7 (3.23%)
Xylene degradation 1 (0.46%)
Vitamin B6 metabolism 4 (1.84%)
Valine, leucine and isoleucine degradation 1 (0.46%)
Valine, leucine and isoleucine biosynthesis 2 (0.92%)
Ubiquinone and other terpenoid-quinone biosynthesis 4 (1.84%)
Tyrosine metabolism 6 (2.76%)
Tryptophan metabolism 6 (2.76%)
Tropane, piperidine and pyridine alkaloid biosynthesis 6 (2.76%)
Toluene degradation 3 (1.38%)
Thiamine metabolism 5 (2.3%)
Terpenoid backbone biosynthesis 2 (0.92%)
Taurine and hypotaurine metabolism 2 (0.92%)
Sulfur metabolism 2 (0.92%)
Styrene degradation 1 (0.46%)
Streptomycin biosynthesis 1 (0.46%)
Starch and sucrose metabolism 2 (0.92%)
Riboflavin metabolism 2 (0.92%)
Pyruvate metabolism 2 (0.92%)
Pyrimidine metabolism 13 (5.99%)
Puromycin biosynthesis 1 (0.46%)
Purine metabolism 20 (9.22%)
Propanoate metabolism 1 (0.46%)
Primary bile acid biosynthesis 1 (0.46%)
Porphyrin and chlorophyll metabolism 4 (1.84%)
Polycyclic aromatic hydrocarbon degradation 2 (0.92%)
Photosynthesis 1 (0.46%)
Phosphonate and phosphinate metabolism 1 (0.46%)
Phenylpropanoid biosynthesis 14 (6.45%)
Phenylalanine, tyrosine and tryptophan biosynthesis 7 (3.23%)
Phenylalanine metabolism 15 (6.91%)
Peptidoglycan biosynthesis 1 (0.46%)
Pentose phosphate pathway 2 (0.92%)
Pentose and glucuronate interconversions 2 (0.92%)
Penicillin and cephalosporin biosynthesis 1 (0.46%)
Pantothenate and CoA biosynthesis 4 (1.84%)
Oxidative phosphorylation 2 (0.92%)
Novobiocin biosynthesis 1 (0.46%)
Nitrogen metabolism 2 (0.92%)
Nicotinate and nicotinamide metabolism 4 (1.84%)
Neomycin, kanamycin and gentamicin biosynthesis 3 (1.38%)
Naphthalene degradation 2 (0.92%)
Monobactam biosynthesis 3 (1.38%)
Microbial metabolism in diverse environments 34 (15.67%)
Methane metabolism 3 (1.38%)
Metabolic pathways 131 (60.37%)
Lysine degradation 7 (3.23%)
Lysine biosynthesis 3 (1.38%)
Linoleic acid metabolism 4 (1.84%)
Isoquinoline alkaloid biosynthesis 3 (1.38%)
Isoflavonoid biosynthesis 5 (2.3%)
Inositol phosphate metabolism 1 (0.46%)
Indole alkaloid biosynthesis 1 (0.46%)
Histidine metabolism 4 (1.84%)
Glyoxylate and dicarboxylate metabolism 6 (2.76%)
Glycosylphosphatidylinositol (GPI)-anchor biosynthesis 3 (1.38%)
Glycine, serine and threonine metabolism 5 (2.3%)
Glycerophospholipid metabolism 15 (6.91%)
Glycerolipid metabolism 1 (0.46%)
Glutathione metabolism 13 (5.99%)
Glucosinolate biosynthesis 6 (2.76%)
Galactose metabolism 3 (1.38%)
Fructose and mannose metabolism 1 (0.46%)
Folate biosynthesis 2 (0.92%)
Flavonoid biosynthesis 40 (18.43%)
Flavone and flavonol biosynthesis 29 (13.36%)
Fatty acid degradation 2 (0.92%)
Fatty acid biosynthesis 1 (0.46%)
Ether lipid metabolism 3 (1.38%)
Drug metabolism - other enzymes 1 (0.46%)
Dioxin degradation 2 (0.92%)
Degradation of aromatic compounds 10 (4.61%)
D-Glutamine and D-glutamate metabolism 2 (0.92%)
D-Arginine and D-ornithine metabolism 1 (0.46%)
D-Alanine metabolism 1 (0.46%)
Cysteine and methionine metabolism 9 (4.15%)
Cyanoamino acid metabolism 6 (2.76%)
Clavulanic acid biosynthesis 1 (0.46%)
Citrate cycle (TCA cycle) 3 (1.38%)
Chlorocyclohexane and chlorobenzene degradation 1 (0.46%)
Carbon metabolism 7 (3.23%)
Carbon fixation pathways in prokaryotes 3 (1.38%)
Carbon fixation in photosynthetic organisms 1 (0.46%)
Carbapenem biosynthesis 3 (1.38%)
C5-Branched dibasic acid metabolism 2 (0.92%)
Butanoate metabolism 4 (1.84%)
Bisphenol degradation 1 (0.46%)
Biotin metabolism 2 (0.92%)
Biosynthesis of vancomycin group antibiotics 1 (0.46%)
Biosynthesis of unsaturated fatty acids 1 (0.46%)
Biosynthesis of terpenoids and steroids 3 (1.38%)
Biosynthesis of siderophore group nonribosomal peptides 2 (0.92%)
Biosynthesis of secondary metabolites 87 (40.09%)
Biosynthesis of plant secondary metabolites 22 (10.14%)
Biosynthesis of plant hormones 9 (4.15%)
Biosynthesis of phenylpropanoids 16 (7.37%)
Biosynthesis of antibiotics 31 (14.29%)
Biosynthesis of ansamycins 1 (0.46%)
Biosynthesis of amino acids 23 (10.6%)
Biosynthesis of alkaloids derived from terpenoid and polyketide 2 (0.92%)
Biosynthesis of alkaloids derived from shikimate pathway 9 (4.15%)
Biosynthesis of alkaloids derived from ornithine, lysine and nicotinic acid 6 (2.76%)
Biosynthesis of alkaloids derived from histidine and purine 8 (3.69%)
Betalain biosynthesis 1 (0.46%)
beta-Alanine metabolism 7 (3.23%)
Benzoxazinoid biosynthesis 1 (0.46%)
Benzoate degradation 6 (2.76%)
Ascorbate and aldarate metabolism 2 (0.92%)
Arginine biosynthesis 5 (2.3%)
Arginine and proline metabolism 15 (6.91%)
Arachidonic acid metabolism 3 (1.38%)
Anthocyanin biosynthesis 10 (4.61%)
Aminobenzoate degradation 9 (4.15%)
Amino sugar and nucleotide sugar metabolism 1 (0.46%)
alpha-Linolenic acid metabolism 4 (1.84%)
Alanine, aspartate and glutamate metabolism 6 (2.76%)
2-Oxocarboxylic acid metabolism 13 (5.99%)
Metabolism
Vibrio cholerae infection 1 (0.46%)
Vancomycin resistance 2 (0.92%)
Salmonella infection 1 (0.46%)
Prion diseases 1 (0.46%)
Pertussis 1 (0.46%)
Pathways in cancer 1 (0.46%)
Pathogenic Escherichia coli infection 3 (1.38%)
Parkinson's disease 6 (2.76%)
Nicotine addiction 2 (0.92%)
Morphine addiction 6 (2.76%)
Insulin resistance 1 (0.46%)
Huntington's disease 1 (0.46%)
Human papillomavirus infection 1 (0.46%)
HTLV-I infection 1 (0.46%)
Endocrine resistance 1 (0.46%)
Dilated cardiomyopathy (DCM) 1 (0.46%)
Cocaine addiction 3 (1.38%)
Choline metabolism in cancer 6 (2.76%)
Chagas disease (American trypanosomiasis) 2 (0.92%)
Central carbon metabolism in cancer 15 (6.91%)
Asthma 1 (0.46%)
Antifolate resistance 4 (1.84%)
Amyotrophic lateral sclerosis (ALS) 2 (0.92%)
Amphetamine addiction 3 (1.38%)
Amoebiasis 2 (0.92%)
Alcoholism 6 (2.76%)
Human Diseases
Sulfur relay system 2 (0.92%)
Aminoacyl-tRNA biosynthesis 14 (6.45%)
Genetic Information Processing
Two-component system 5 (2.3%)
Sphingolipid signaling pathway 3 (1.38%)
Ras signaling pathway 1 (0.46%)
Rap1 signaling pathway 1 (0.46%)
Plant hormone signal transduction 1 (0.46%)
PI3K-Akt signaling pathway 1 (0.46%)
Phosphotransferase system (PTS) 3 (1.38%)
Phospholipase D signaling pathway 2 (0.92%)
Neuroactive ligand-receptor interaction 11 (5.07%)
mTOR signaling pathway 2 (0.92%)
MAPK signaling pathway 1 (0.46%)
Hedgehog signaling pathway 1 (0.46%)
FoxO signaling pathway 2 (0.92%)
cGMP-PKG signaling pathway 6 (2.76%)
cAMP signaling pathway 8 (3.69%)
Calcium signaling pathway 1 (0.46%)
Apelin signaling pathway 1 (0.46%)
AMPK signaling pathway 9 (4.15%)
ABC transporters 20 (9.22%)
Environmental Information Processing
Histamine H2/H3 receptor agonists/antagonists 1 (0.46%)
Drug Development
Benzoic acid family 1 (0.46%)
Quorum sensing 1 (0.46%)
Oocyte meiosis 1 (0.46%)
Meiosis - yeast 1 (0.46%)
Gap junction 3 (1.38%)
Ferroptosis 6 (2.76%)
Cell cycle - yeast 1 (0.46%)
Biofilm formation - Vibrio cholerae 2 (0.92%)
Biofilm formation - Pseudomonas aeruginosa 1 (0.46%)
Biofilm formation - Escherichia coli 1 (0.46%)
Autophagy - animal 3 (1.38%)
Cellular Processes
0 4 8 12 18 24 30 36 42 48 54 60
Percent (%)

Figure S4. Differential metabolite KEGG classification chart

Note: The ordinate is the name of the KEGG metabolic pathway, and the abscissa is the number of metabolites annotated to the pathway and its proportion to the total number of metabolites annotated.

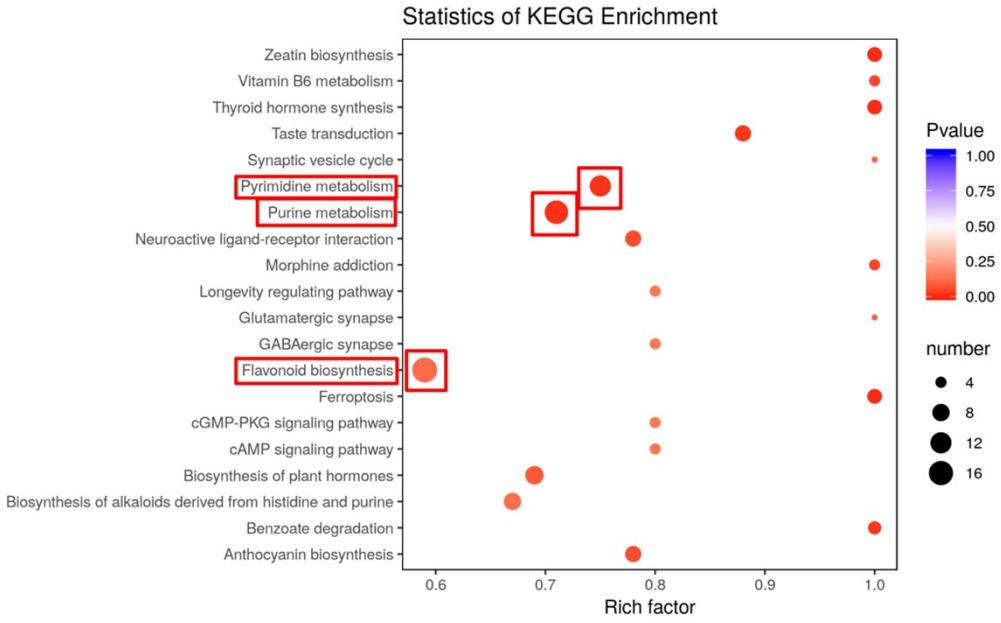

Figure S5. KEGG enrichment analysis of differentially accumulating metabolites between succulent stem and inflorescence.

Note: The abscissa represents the rich factor corresponding to each channel, the ordinate is the channel name, and the color of the point is *p*-value. The redder, the more significant the enrichment. The size of the dot represents the number of different metabolites enriched.

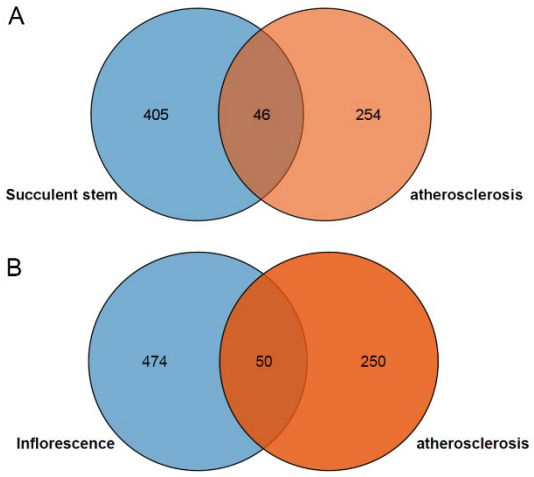

Figure S6. Common genes of succulent stem compounds, inflorescence compounds, and atherosclerosis disease. (A) Common genes of succulent stem compounds and atherosclerosis disease. (B) Common genes of inflorescence compounds and atherosclerosis disease.

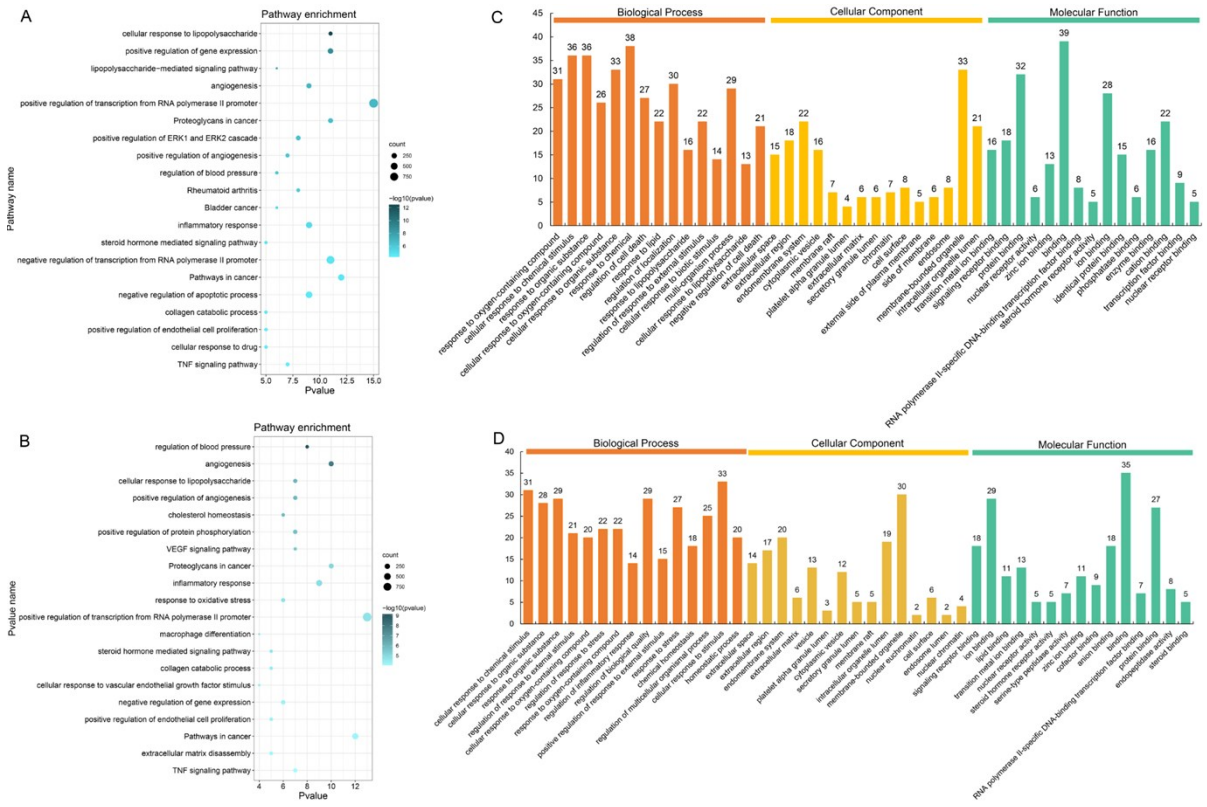

Figure S7. KEGG and GO enrichment analysis of succulent stem and inflorescence. (A) KEGG enrichment analysis of the target genes of the succulent stem by DAVID database. (B) KEGG enrichment analysis of the target genes of inflorescence by DAVID database. (C) The enrichment analysis in biological processes, cellular components, and molecular functions of 39 identified target proteins of the succulent stem by STRING database. (D) The enrichment analysis in biological processes, cellular components, and molecular functions of 36 identified target proteins of inflorescence by STRING database.
Note: Counts refer to the number of the enriched genes.

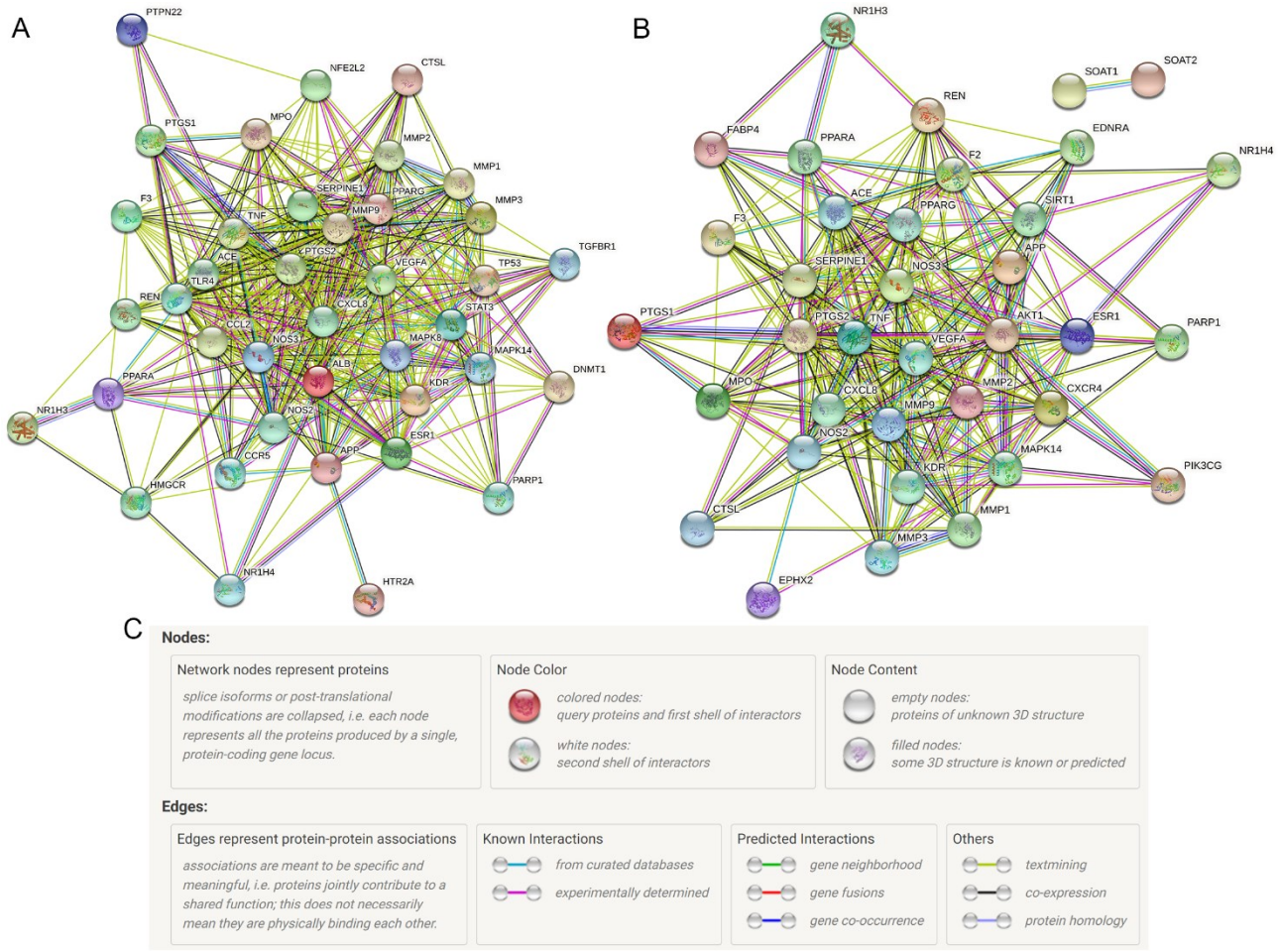

Figure S8. Protein-Protein interaction (PPI) network. (A) PPI network of succulent stem exported from the STRING database. (B) PPI network of inflorescence exported from the STRING database. (C) Annotations for the nodes and edges in the PPI network.

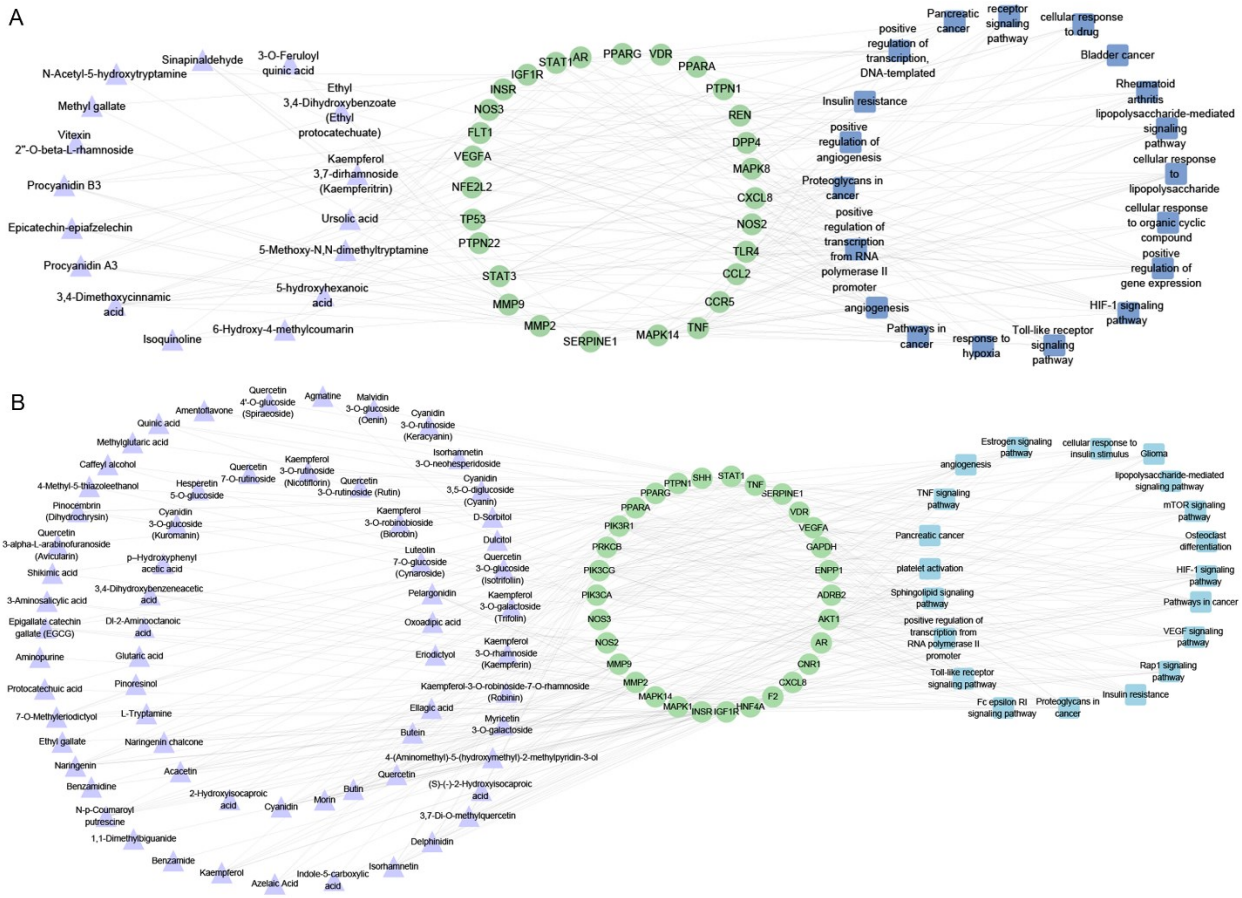

Figure S9. Compound-protein target-pathway map of succulent stem and inflorescence in diabetes. (A) Compound-protein target-pathway map of the succulent stem. (B) Compound-protein target-pathway map of the inflorescence.

Note: Purple triangles represent compounds, green circles represent protein targets, and blue squares represent pathways.

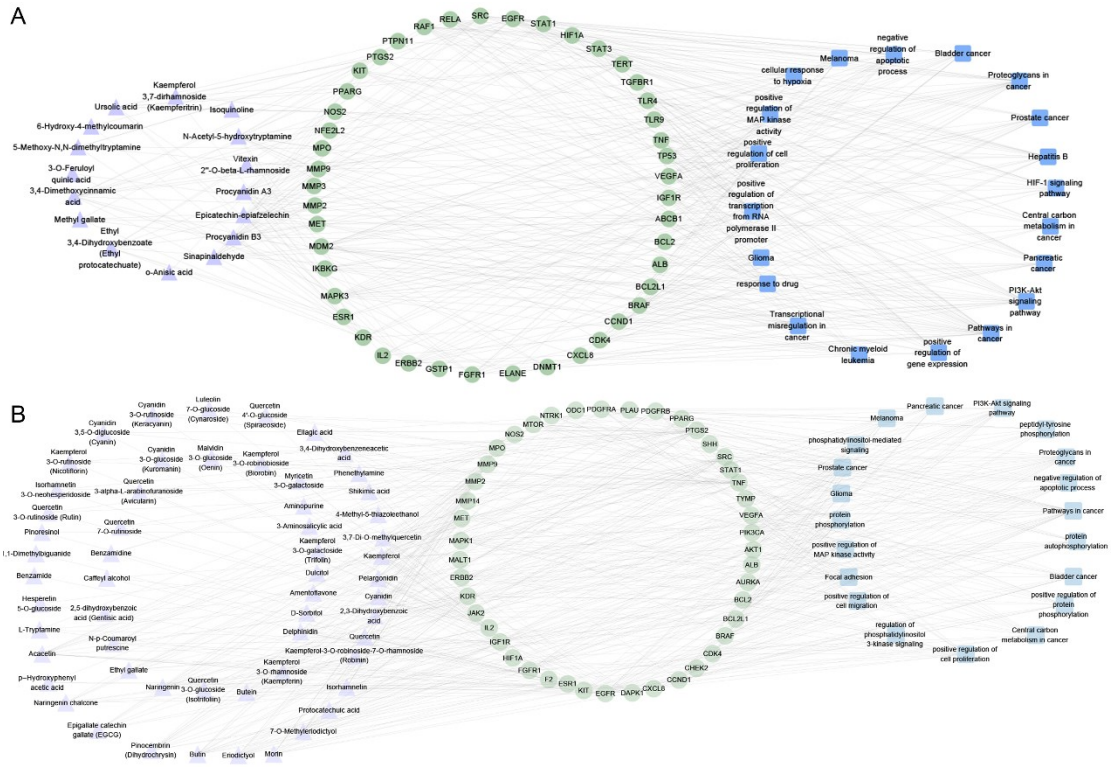

Figure S10. Compound-protein target-pathway map of succulent stem and inflorescence in gastric ulcer. (A) Compound-protein target-pathway map of the succulent stem. (B) Compound-protein target-pathway map of the inflorescence.

Note: Purple triangles represent compounds, green circles represent protein targets, and blue squares represent pathways.

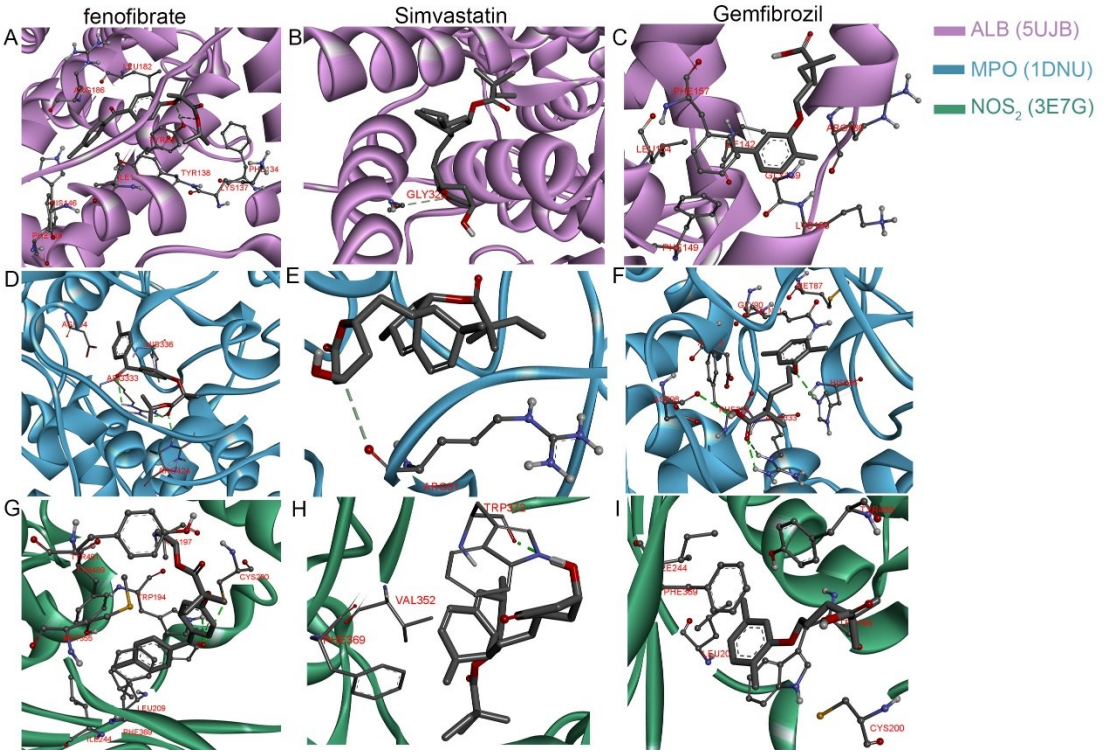

Figure S11. Molecular docking results of the positive drug. (A) The action mode of ALB and

fenofibrate; (B) The action mode of ALB and Simvastatin; (C) The action mode of ALB and gemfibrozil; (D) The action mode of MPO and fenofibrate; (E) The action mode of MPO and Simvastatin; (F) The action mode of MPO and gemfibrozil; (G) The action mode of NOS_2 and fenofibrate; (H) The action mode of NOS_2 and Simvastatin; (I) The action mode of NOS_2 and gemfibrozil.